 CMES, vol.13, no.2, pp.91-101, 2006

Meshfree Solution of Q-tensor Equations of Nematostatics Using the MLPG Method

Radek Pecher[1], Steve Elston, and Peter Raynes

Abstract: Meshfree techniques for solving partial differential equations in physics and engineering are a powerful new alternative to the traditional mesh-based techniques, such as the finite difference method or the finite element method. The elimination of the domain mesh enables, among other benefits, more efficient solutions of nonlinear and multi-scale problems. One particular example of these kinds of problems is a Q-tensor based model of nematic liquid crystals involving topological defects.

This paper presents the first application of the meshless local Petrov-Galerkin method to solving the Q-tensor equations of nematostatics. The theoretical part introduces the Landau – de Gennes free-energy functional and its meshfree minimisation subject to the given boundary constraints. The theory is followed by two example models with simple distortion profiles, including a twisted chiral nematic. The resulting profiles exhibit large local gradients and a high degree of continuity even for few semi-regularly distributed nodes, indicating the high accuracy of the meshfree approach used.

keyword: Nematic liquid crystals, Meshfree modelling, Tensor order parameter, Topological defects, Meshless local Petrov-Galerkin method, MLPG

1 Introduction

Numerical modelling of physical processes is responsible for many advances in science and technology. Continuum-based *partial differential equations* (PDEs), describing physical processes at the macroscopic scale, have been numerically solved over the last half-century almost exclusively by using some type of mesh-based method: *finite difference method* (FDM), *control volume method* (CVM), *finite element method* (FEM), *boundary element method* (BEM), etc. In general, all of these methods (including BEM) require that the spatial domain of interest be divided into a number of small cells with strict relations between the solution nodes. Since the cell sizes and shapes directly control the discretisation error, the mesh density and topology should closely conform to the variation in the solution quantity. This is ensured by adaptively refining the mesh and therefore coping with the inter-nodal constraints, which is both tricky and costly, especially in a three-dimensional space.

A strong contender to complement the mesh-based methods is a newly emerging family of so-called *meshless* or *meshfree methods* for solving PDEs. In particular, the *meshless local Petrov-Galerkin* (MLPG) method, introduced by Atluri and Zhu [Atluri and Zhu (1998)], is a very promising new alternative to the FEM and may soon appear in commercial codes. As a truly meshless technique, the MLPG is formulated by means of a set of nodes arbitrarily distributed throughout the domain of interest. The nodes are all independent of each other and can be conveniently added or removed according to the solution requirements. In addition to the straightforward *h*-refinement, the *p*-refinement is also more easily applied in MLPG than in FEM. Nevertheless, the MLPG solution is smooth even with a linear polynomial basis, unlike the solution of linear finite elements. For these and other reasons, the MLPG is thought to be more accurate than the FEM, and comparisons of results from the two methods confirm this opinion (see e.g. [Atluri and Shen (2002)] p.209, [Liu (2003)] p.236). The other obvious practical benefit of eliminating the domain mesh is the savings in manpower and software needed for designing high-quality meshes.

The problems particularly suited for a meshfree solution approach are those posing major difficulties to the mesh-based methods: for example, problems involving large local gradients and singularities, multi-scale problems, strongly nonlinear problems, moving boundary problems, etc. The modelling of *liquid crystal* (LC) devices combines several categories of such "difficult problems",

[1] Department of Engineering Science, University of Oxford, Parks Road, Oxford, OX1,3PJ, U.K. tel: +44 (0)1865 273044, fax: +44 (0)1865 273905,email:radek.pecher@eng.ox.ac.uk

mainly due to the occurrence of *topological defects* that can play an important role in the switching of some devices.

This paper is divided into six sections including this introduction. Section 2 presents a brief overview of nematic liquid crystals, their mathematical description and the equations of static equilibrium in an LC-device. Section 3 explains the conversion of the governing PDE of Section 2 into its approximate integral form known as the *discrete local weak form* (DLWF). The DLWF formulation is the first step of the MLPG solution procedure further described in Section 4. The theory is followed by the results of two solved example problems summarised in Section 5. Finally, Section 6 reviews the main findings of Section 5 and suggests future extensions of the current work.

2 Equations of Nematostatics

Nematic liquid crystals are liquid compounds that exhibit an increased *orientational order* among their molecules as compared to isotropic liquids. The quantity describing the amount of orientational order at any given point in space and time is called the *scalar order parameter* (SOP), $S(\mathbf{x},t)$. The preferred average direction of a group of elongated molecules at $\{\mathbf{x},t\}$ is represented by a unit vector $\hat{\mathbf{n}}(\mathbf{x},t)$ called the *director*. If θ_m is the angle between the director and the long axis of each of the molecules, see Figure 1, then the scalar order parameter may be expressed [de Gennes and Prost (1993)] as the spatial – temporal continuum average

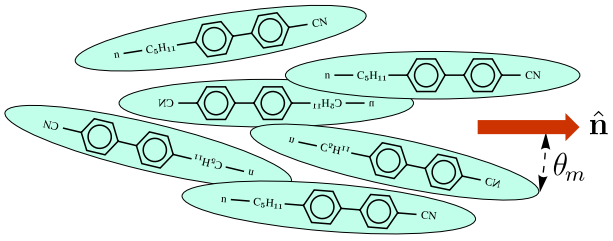

Figure 1 : Group of molecules of nematic LC compound 5CB.

$$S = \tfrac{1}{2}\left\langle 3\cos^2\theta_m - 1\right\rangle , \qquad S \in [-\tfrac{1}{2}, 1] , \tag{1}$$

based on quadrupolar interactions between the molecules.

A more general and compact description of an LC-state, rather than the pair $\{S,\hat{\mathbf{n}}\}$, is in terms of the *tensor order parameter* (TOP), $\mathbf{Q}(\mathbf{x},t)$, also known as the Q-tensor:

$$\begin{aligned}\mathbf{Q} &= S_1\,(\hat{\mathbf{n}}\otimes\hat{\mathbf{n}}) + S_2\,(\hat{\mathbf{m}}\otimes\hat{\mathbf{m}}) - \tfrac{1}{3}(S_1+S_2)\,\mathbf{I} \\ &= \begin{pmatrix} q_1 & q_2 & q_3 \\ q_2 & q_4 & q_5 \\ q_3 & q_5 & -q_1-q_4 \end{pmatrix} .\end{aligned} \tag{2}$$

$\mathbf{Q}$ is a symmetric traceless tensor with five independent components q_i in the 3D-space. It allows for *biaxiality* of the LC-system by including two SOP – director pairs, namely $\{S_1,\hat{\mathbf{n}}\}$ and $\{S_2,\hat{\mathbf{m}}\}$.

Any change of the director distortion is associated with an increase of energy, and therefore the lowest energy state normally corresponds to the uniform director field. This is not the case, however, for the so-called *chiral nematic* or *cholesteric* liquid crystals which spontaneously twist around an axis normal to their director field, see Figure 2. The resulting helical structure is mathematically described in terms of the wave-vector q_0 also known as the *permanent twist*. If q_0 is zero, the liquid crystals are called *achiral nematic* or simply nematic.

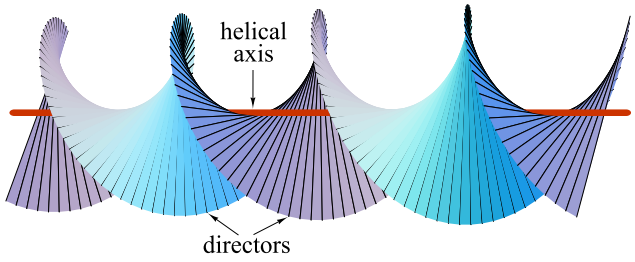

Figure 2 : Helical structure of chiral nematic LCs.

The excess *free-energy density* (FED) corresponding to the spatial variation of the scalar director field may be expressed [Oseen (1933), Frank (1958)] as

$$\begin{aligned}F_{\mathrm{e}} \;=\; & \frac{k_{11}}{2}(\nabla\cdot\hat{\mathbf{n}})^2 \;+\; \frac{k_{22}}{2}(\hat{\mathbf{n}}\cdot\nabla\times\hat{\mathbf{n}} - q_0)^2 \\ & + \frac{k_{33}}{2}(\hat{\mathbf{n}}\times\nabla\times\hat{\mathbf{n}})^2 \\ & + \frac{k_{22}+k_{24}}{2}\Big[\mathrm{tr}\Big((\nabla\hat{\mathbf{n}})^2\Big) - (\nabla\cdot\hat{\mathbf{n}})^2\Big]\end{aligned} \tag{3}$$

and is called the *elastic* FED. The material constants k_{11}, k_{22}, k_{33} and k_{24} relate to the *splay*, *twist*, *bend* and *saddle*

splay, respectively. This purely $\hat{\mathbf{n}}$-based form of F_e, also referred to as *Frank-Oseen elastic energy density*, does not take into account biaxiality and variation of the order parameter.

The more general, $\mathbf{Q}$-based form of the elastic FED, which does allow for biaxiality and SOP-variation, and therefore more rigorously characterises topological defects, is the following sum [Berreman and Meiboom (1984), Mori, Gartland, Kelly, and Bos (1999)] of six terms:

$$
\begin{aligned}
F_e &= \sum_{i=1}^{6} \tfrac{1}{2} L_i G_i, \\
L_1 &= \frac{1}{6 S_{eq}^2}(k_{33}-k_{11}+3k_{22}), G_1 = \sum_{i,j,k} \frac{\partial Q_{ij}}{\partial x_k}\frac{\partial Q_{ij}}{\partial x_k}, \\
L_2 &= \frac{1}{S_{eq}^2}(k_{11}-k_{22}-k_{24}), G_2 = \sum_{i,j,k} \frac{\partial Q_{ij}}{\partial x_j}\frac{\partial Q_{ik}}{\partial x_k}, \\
L_3 &= \frac{1}{S_{eq}^2} k_{24}, G_3 = \sum_{i,j,k} \frac{\partial Q_{ij}}{\partial x_k}\frac{\partial Q_{ik}}{\partial x_j}, \\
L_4 &= \frac{2}{S_{eq}^2} q_0 k_{22}, G_4 = \sum_{i,j,k,l} \varepsilon_{ijk} Q_{il} \frac{\partial Q_{jl}}{\partial x_k}, \\
L_5 &= \frac{3}{2 S_{eq}^2} q_0^2 k_{22}, G_5 = \sum_{i,j} Q_{ij} Q_{ij}, \\
L_6 &= \frac{1}{2 S_{eq}^3}(k_{33}-k_{11}), G_6 = \sum_{i,j,k,l} Q_{ij} \frac{\partial Q_{kl}}{\partial x_i}\frac{\partial Q_{kl}}{\partial x_j},
\end{aligned}
\qquad (4)
$$

where S_{eq} is the bulk equilibrium uniaxial scalar order parameter at the temperature of k-constants' measurement, here simply referred to as the equilibrium SOP. The elastic constants L_i are more-or-less temperature independent, whereas the temperature dependence of k-constants is dictated by that of the order parameter.

Equation (4) differs from [Mori, Gartland, Kelly, and Bos (1999)] by the extra term $L_5 G_5$ which has been added in order to properly model chiral nematics in terms of $\mathbf{Q}$. It is important to notice that the formulation of Eq. (4) is a version of the $\mathbf{Q}$-based F_e that exactly simplifies to the $\hat{\mathbf{n}}$-based F_e of Eq. (3) for $S_1 = S_{eq}$ and $S_2 = 0$.

Since the (nonconservative) scalar order parameter is allowed to vary in the Q-tensor approach, its magnitude itself should also affect the total energy of the LC-system. Landau [Landau and Lifshitz (1980)] introduced the corresponding free-energy density, called *thermotropic*,

$$
F_t = \frac{a(\Delta T)}{2}\mathrm{tr}(\mathbf{Q}^2) + \frac{b}{3}\mathrm{tr}(\mathbf{Q}^3) + \frac{c}{4}\left[\mathrm{tr}(\mathbf{Q}^2)\right]^2 , \qquad (5)
$$

which models the transition between the nematic and isotropic states as a function of temperature difference $\Delta T = T - T^*$ from the temperature T^* at which the isotropic state is no longer stable. If S denotes the uniaxial SOP S_1, while S_2 is assumed zero, the global minimiser S_{eq} of the function $F_t(S)$ for any non-positive value of ΔT is obtained from the material constants a, b and c as

$$
S_{eq} = \frac{-b+\sqrt{b^2-24ac}}{4c} . \qquad (6)
$$

Figure 3 shows four $F_t(S)$ curves for various ΔT's and the following values[2] of the thermotropic constants:

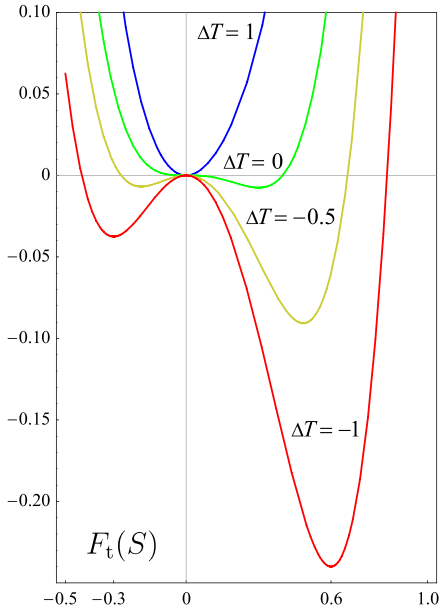

Figure 3 : Isothermal curves $F_t(S)$ for various values of ΔT.

$$
a = 3\Delta T , \qquad b = -15 , \qquad c = 25 . \qquad (7)
$$

The particular curve corresponding to $\Delta T = -1$, for which $S_{eq} = 0.6$, represents the isothermal characteristic $F_t(S)$ of a stable nematic state chosen for the actual computations in Section 5.

The total free-energy density is a sum of the thermotropic and elastic contributions,

$$
F(\mathbf{Q}, \nabla\mathbf{Q}, \mathbf{x}, t) = F_t + F_e , \qquad (8)
$$

[2] Throughout this paper, if not specified otherwise, all quantities are defined as dimensionless, based on a characteristic length at the nanometres scale.

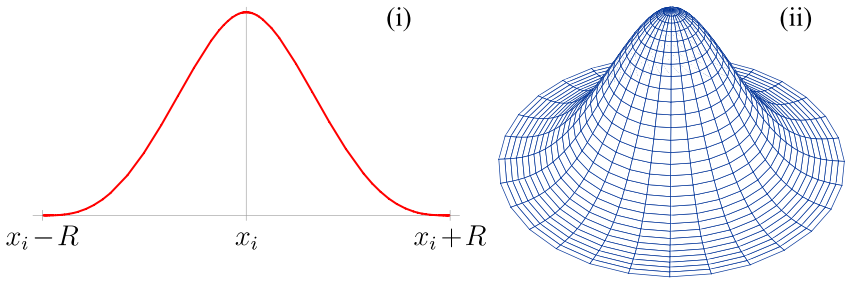

Figure 4 : Quartic-spline weight function in (i) 1D and (ii) 2D.

while omitting other contributions, such as those related to externally applied fields or device surface treatments which are not considered in this paper.

The free energy of an LC-device, also referred to as the *Landau – de Gennes free-energy functional*, is the integral

$$\mathcal{F} = \int_\Omega F(\mathbf{Q}, \nabla\mathbf{Q}, \mathbf{x}, t)\, \mathrm{d}\Omega \tag{9}$$

where Ω is the global spatial domain of interest.

The Dirichlet-type boundary condition assumed for the entire boundary Γ of the domain Ω is simply

$$\mathbf{Q}(\mathbf{x}) = \overline{\mathbf{Q}}(\mathbf{x})\,, \qquad \mathbf{x} \in \Gamma\,. \tag{10}$$

That corresponds to an infinite anchoring strength of the liquid crystal alignment in the preferred directions at the device walls, a case known as *strong anchoring*.

Static equilibrium of the LC-system under consideration is found by minimising the functional of Eq. (9) subject to the constraint of Eq. (10); this is equivalent to solving the following Euler equations:

$$\begin{aligned} &\nabla\cdot\mathbf{g}_i(q_j, \nabla q_j, \mathbf{x}) \;+\; f_i(q_j, \nabla q_j, \mathbf{x}) \;=\; 0\,, \\ &\quad \mathbf{x} \in \Omega\,, \qquad i = 1, \ldots, 5\,, \\ &\quad f_i = \frac{\partial F}{\partial q_i}\,, \qquad \mathbf{g}_i = -\frac{\partial F}{\partial(\nabla q_i)}\,. \end{aligned} \tag{11}$$

Functions f and $\mathbf{g}$ may be called the "*internal-force function*" and the "*gradient function*", respectively. Equation (11) represents five nonlinear second-order partial differential equations describing the LC-device problem to be solved in terms of five unknown components q_i of the tensor order parameter $\mathbf{Q}$. The associated boundary condition, Eq. (10), is rewritten using the q_i-notation as

$$q_i(\mathbf{x}) = \overline{q_i}(\mathbf{x})\,, \qquad \mathbf{x} \in \Gamma\,, \qquad i = 1, \ldots, 5\,. \tag{12}$$

3 Discrete Local Weak Form of PDE

The initial step in solving the partial differential equations (11) and the boundary conditions (12) using the meshfree procedure of MLPG is the formulation of the corresponding approximate integral equation. In order to find the approximate numerical solutions $\tilde{q}_i$ of the governing equations, for any suitable approximation scheme specified later, the domain integral of the *weighted PDE-residual* is forced to zero, as follows[3]

$$\int_\Omega w(\nabla\cdot\tilde{\mathbf{g}} + \tilde{f})\, \mathrm{d}\Omega \;=\; 0\,. \tag{13}$$

In MLPG, the weight function w, or the so-called *test function*, is different from the *trial function* used to approximate the solution q. Such an approach is known within the FEM community as the *Petrov-Galerkin method* (giving MLPG its name) and leads to non-symmetric solution matrices.

The principal role of the test function w in Eq. (13) is to restrict the region where the PDE-residual is forced to zero to a small section of the global domain Ω. If also the trial function has a similar local character, the resulting solution matrix is guaranteed to be sparse, which is a crucial efficiency requirement for any PDE solution method. From a variety of suitable candidates, bell-shaped functions [Liu (2003)] provide the most "natural" and optimum weighting. Our choice is the *quartic-spline* weight function

$$w(r \equiv \|\mathbf{x} - \mathbf{x}_i\|) \;=\; \begin{cases} (1 + 3\,r/R)(1 - r/R)^3 & \text{for } r < R \\ 0 & \text{for } r \geq R \end{cases} \tag{14}$$

[3] From this point onwards, the five equation – unknown pairs in Eqs. (11) and (12) will be treated jointly as a single pair without specifying its index i.

depicted in Fig. 4.

Upon integrating the first term in Eq. (13) by parts and taking into account the local property of the suitably chosen test function w, the integral equation becomes

$$\int_{S_N(\mathbf{x}_i,R_i)} w_i \tilde{f}\,\mathrm{d}\omega - \int_{S_N(\mathbf{x}_i,R_i)} \nabla w_i \cdot \tilde{\mathbf{g}}\,\mathrm{d}\omega = 0 \qquad \text{for node } i \tag{15}$$

where w_i is the weight function related to node i positioned at $\mathbf{x}_i$. Eq. (15) is based on the assumption that the local domain of nonzero w_i is an N-sphere, N being the number of spatial dimensions. The surface integral from the integration by parts vanishes because of the zero weight w_i at the N-sphere surface. Similarly, the domain of integration reduces from the global domain Ω to the local domain $S_N(\mathbf{x}_i,R_i)$, or the N-sphere of radius R_i centred at point $\mathbf{x}_i$.

Eq. (15) is the discrete local weak form of the partial differential equation (11). "Discrete" because of the approximations based on nodes (the discrete representation of continuous space), "local" because of the local integration domain, and "weak" because the differentiability requirement on $\tilde{\mathbf{g}}$ has been weakened by shifting the divergence from $\tilde{\mathbf{g}}$ to w, cf. Eqs. (13) and (15).

It should be added that certain DLWF formulations found in the MLPG literature further contain additional terms related to the implementation of the Dirichlet-type boundary conditions. We prefer the more efficient and simpler approach of [Li, Shen, Han, and Atluri (2003)] mentioned in the following section.

4 Solution Procedure of MLPG1

The meshless local Petrov-Galerkin method solves the governing partial differential equation, Eq. (11), in the form of the corresponding approximate integral equation, Eq. (15), the discrete local weak form of the PDE. The solution quantity, q in this case, is approximated by means of the so-called *moving least squares* (MLS) method [Breitkopf, Rassineux, Touzot, and Villon (2000)], which is a powerful data-fitting technique based on a set of nodes arbitrarily distributed within an N-dimensional space. Local character and fitting smoothness of the MLS are ensured by weighting the contributions from all the nodes via a suitable function, such as the quartic spline of Eq. (14). In this paper, the same quartic-spline weight function is used both as the test function w_i in Eq. (15) and as the MLS-weight of the trial function Ψ_j of the solution approximation

$$\tilde{q}(\mathbf{x}) = \sum_{j=1}^{M} \Psi_j(\mathbf{x})\,\tilde{q}_j\,. \tag{16}$$

This choice corresponds to the original version of the MLPG, referred to as MLPG1 [Atluri and Shen (2002)]. In Eq. (16), M is the number of nodes covered by the so-called *support domain* representing a nonzero MLS-weight for any given reference point $\mathbf{x}$, and $\tilde{q}_j$ are the *nodal parameters* of the MLS-based solution approximation.

The actual solution procedure consists of evaluating Eq. (15) consecutively for all, say K, nodes inside the global spatial domain Ω, thereby generating a system of K nonlinear algebraic equations[4] for K unknowns $\tilde{q}_k$:

$$h_k(\tilde{q}_1,\tilde{q}_2,\ldots,\tilde{q}_{K+L}) = 0\,, \quad \mathbf{x}_k \in \Omega\,, \qquad k = 1,\ldots,K\,. \tag{17}$$

Efficient evaluation of the two integrals in Eq. (15) is achieved by applying the specialized Gaussian cubature formulae of [Pecher (2005)] preventing a severe loss of accuracy associated with the mapping between radial and Cartesian coordinates when using the standard quadrature formulae.

The remaining L unknowns $\tilde{q}_l$ corresponding to all the nodes on the global boundary Γ are obtained by directly assigning the boundary condition (12) to the solution approximation (16) as

$$\sum_{j=1}^{M} \Psi_j(\mathbf{x}_l)\,\tilde{q}_j - \overline{q}(\mathbf{x}_l) = 0\,, \qquad \mathbf{x}_l \in \Gamma\,, \qquad l = 1,\ldots,L\,. \tag{18}$$

This generalised assignment easily overcomes the problem with non-interpolating nature of the MLS: $\Psi_j(\mathbf{x}_l) \neq \delta_{jl}$.

The direct assignment of the Dirichlet-type boundary condition through all L nodes on Γ, see Eq. (18), simplifies and improves the DLWF formulation to that of Eq. (15) for all K nodes inside Ω under one strict condition: The global boundary Γ must not intersect the local

[4] Although generally dependent on all unknowns $\tilde{q}_i$, including those of the L boundary nodes, the system of equations has a sparse Jacobian matrix due to the local character of the involved test and trial functions.

Table 1 : Optimum numbers of support nodes, M in Eq. (16), in N spatial dimensions and for order O of the MLS polynomial basis

$N=2$		$N=3$	
$O=1$	$O=2$	$O=1$	$O=2$
7	14	13	32

integration domain of any internal node k:

$$\Gamma \cap \bigcup_{k=1}^{K} S_N(\mathbf{x}_k, R_k) \;=\; \emptyset \,. \tag{19}$$

This can be easily ensured [Li, Shen, Han, and Atluri (2003)] by reducing the domain radius R_k accordingly. Such a strategy is justified even for nodes very close to the boundary due to the following reason:

Statement 1 *Both the density of the nodes' distribution and the size of the local integration domain should proportionally correspond to the variation of the solution quantity.*

Our computer implementation of Eqs. (17) and (18) sets the radius R_k of the N-sphere $S_N(\mathbf{x}_k, R_k)$ to the average distance between $\mathbf{x}_k$ and its $N+1$ closest nodes. This is followed by a possible adjustment of R_k for points $\mathbf{x}_k$ close to the global boundary in order to satisfy Eq. (19).

In a somewhat similar spirit, the size of the MLS support domain of a reference point $\mathbf{x}$, namely the radius R in Eq. (14), is coded in our software *LCQuest*[1] as the distance to the $(M+1)$th node closest to $\mathbf{x}$. The parameter M in Eq. (16) is thus fixed for all points $\mathbf{x}$, while the support domain radius R, implicitly defining the trial functions Ψ_j [Pecher (2005)], varies according to the local density of the nodes' distribution. The optimum value of M has been found by a thorough analysis of symmetries in various regular distributions of nodes in both 2D and 3D and for both linear and quadratic polynomial bases of the MLS, as listed in Table 1. It is perhaps no coincidence that these values correspond to the expression $N\binom{N+O}{N}+O$, since $\binom{N+O}{N}$ represents the number of monomials up to order O in N-D.

[1] More details about the software can be found at http://www.LCQuest.org/.

The primary advantage of the fixed-M approach is an increased code efficiency due to eliminating all overhead instructions associated with variable-size arrays. Today's highly optimising compilers can unroll fixed-count loops, heavily inline code and perform other optimisations based on the predetermined size of arrays. An even higher level of code performance and flexibility can be further achieved by employing recent advances in the *object-oriented numerics*, especially the so-called *expression templates* parameterised in terms of M.

5 Solved Example Problems

This section summarises the main results of two solved example problems. Both problems represent a nematic liquid crystal device with a unit-square domain in 2D (i.e., assuming no variations along the z-axis normal to the domain). A full-3D Q-tensor field, Eq. (2), is obtained by solving Eqs. (17) and (18) using the procedure described in Section 4 with the following specifications: $K+L=576$, $M=14$ (i.e., $N=2$, $O=2$), Gaussian cubature points: 4 (or $m=2$, see [Pecher (2005)]), relative tolerance of the Newton-Krylov solver: 10^{-8}. The distribution of nodes was set up by randomly perturbing a 24×24 point-lattice in both directions by 10% of the inter-nodal distance. The total number of Newton steps taken by the solver was five in both cases and the entire computation of each problem took less than a minute on a single Intel ® Xeon 3GHz processor PC running Linux 9 and GNU gcc 3.4.

The thermotropic constants of the (fictitious) liquid crystal material considered in Example 2 are those given by Eq. (7) with $\Delta T=-1$, see also Fig. 3. Similar values, only multiplied by 100, are assigned to Example 1 in order to reduce the size of the resulting topological defect and hence make the problem numerically more demanding.

The elastic constants and chirality of the LC-material for both problems are chosen as follows:

$$\begin{aligned} &k_{11}=k_{22}=k_{33}=1\,,\\ &k_{24}=0\,,\\ &q_0=\begin{cases} 0 & \text{in Example 1}\\ -\frac{\pi}{2} & \text{in Example 2}\end{cases}. \end{aligned} \tag{20}$$

This corresponds to the so-called "*one-constant approximation*" leading to simplifications in Eqs. (3) and (4). Al-

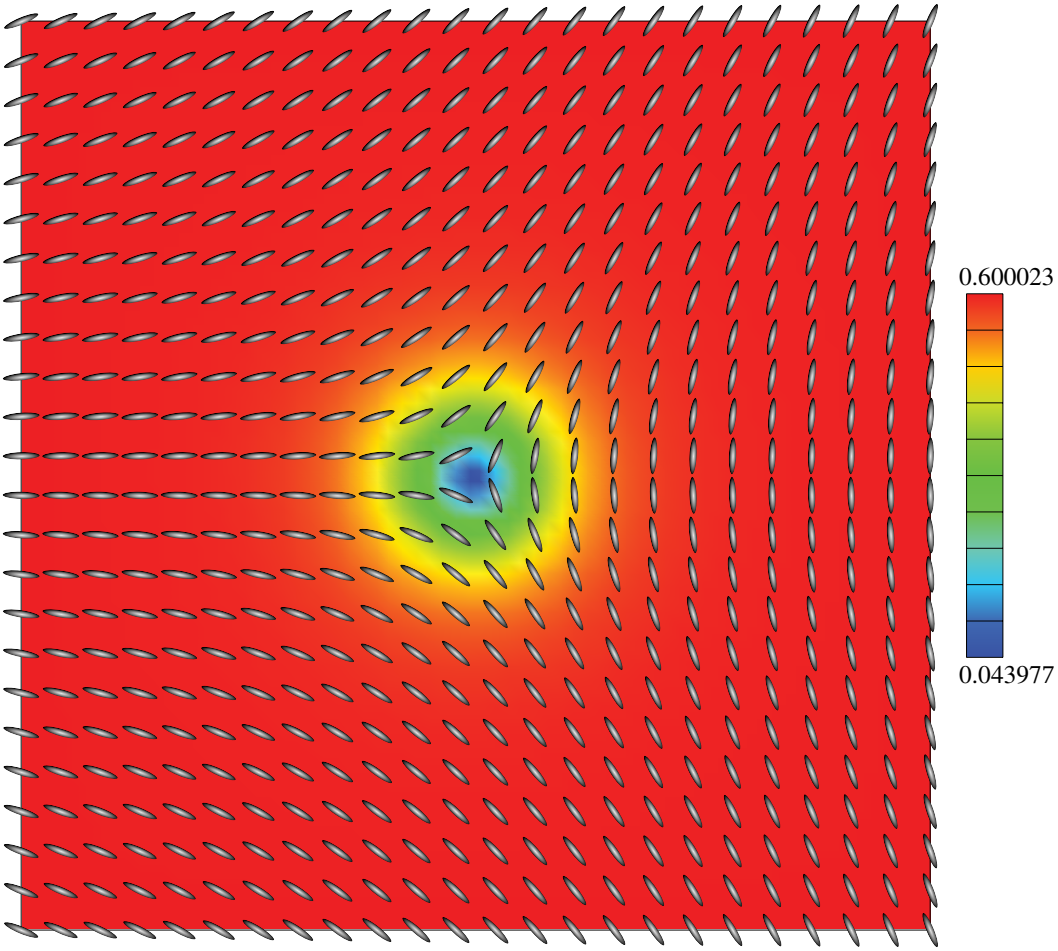

Figure 5 : Resulting profiles of S_1 and $\hat{\mathbf{n}}$ obtained by solving Example 1.

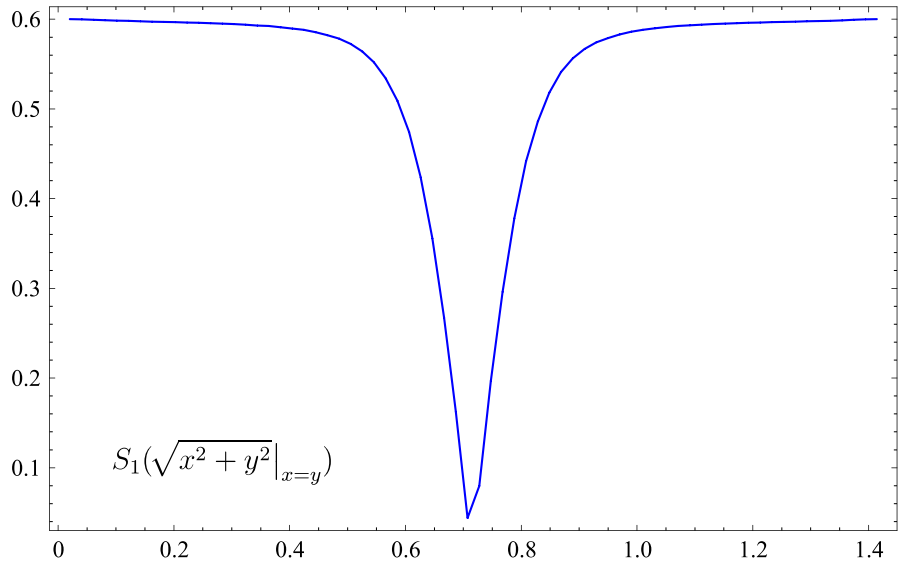

Figure 6 : Diagonal cross-section profile of S_1 from Example 1.

though the software LCQuest implements the fully general form of Eq. (4), the choice of values as in Eq. (20) makes it easier to analyse and verify the modelling results.

The results are presented in the form of combined density – vector plots[5]. The density plot illustrates the scalar order parameter, S_1 or S_2, whereas the vector plot depicts the corresponding director, i.e. $\hat{\mathbf{n}}$ or $\hat{\mathbf{m}}$. The vector plot uses shaded ellipses in an attempt to imitate prolate spheroids in 3D oriented along the directors (note: no polarity is indicated due to the equivalences $\hat{\mathbf{n}} = -\hat{\mathbf{n}}$ and $\hat{\mathbf{m}} = -\hat{\mathbf{m}}$). The data sampling for both plots is carried out on a regular point-lattice of size 70×70 for the density plot and 24×24 for the vector plot. Thus, the sampling in the vector plot is the same as the distribution of nodes for both examples, while disregarding the imposed random perturbations of the latter.

The rest of this section presents the descriptions and results of the two examples.

Example 1 The first example demonstrates the occurrence of a topological defect or "*disclination*" of strength $-\frac{1}{2}$ (see e.g. [de Gennes and Prost (1993)] p.163+) as a result of the following boundary conditions:

$$\begin{aligned} &S_1 = S_{\text{eq}}\,, \qquad S_2 = 0\,, \qquad \hat{\mathbf{n}} = (\cos\phi, \sin\phi, 0)\,, \\ &\hat{\mathbf{m}}\text{: undefined}, \quad \phi = -\tfrac{1}{2}\tan^{-1}\frac{1-2y}{1-2x}\,, \\ &(x,y) \in \partial([0,1]\times[0,1])\,. \end{aligned} \tag{21}$$

Figure 5 shows the resulting profiles of the pair $\{S_1, \hat{\mathbf{n}}\}$. The corresponding pair $\{S_2, \hat{\mathbf{m}}\}$, not shown here for its redundancy, exhibits the same shape as the S_1-variation, only scaled to interval $[-0.278, 0]$, and a uniform director field: $\hat{\mathbf{m}} = (0,0,1)$. The results clearly show a singularity in the centre of the problem domain where the director abruptly changes and the uniaxial SOP S_1 approaches a zero value, i.e. the liquid crystal "melts". S_1 in the defect core, however, never reaches zero and, at the same time, S_2 becomes minimum there as well, i.e. the nematic becomes highly biaxial in the centre of a half-strength disclination, which was analytically predicted by Schopohl and Sluckin [Schopohl and Sluckin (1987)]. The apparent fluctuations of S_1 near the defect's core are caused by the visualisation of the large gradients. The actual solution is in fact very smooth, as is evident from the cross-section profile in Figure 6 along the domain diagonal $x = y$.

[5] Each plot is the actual PostScript output from LCQuest, and hence more details can be viewed by zooming in.

Example 2 The second example investigates the effect of chirality, or permanent twist, of a cholesteric liquid crystal subjected to an imposed twist along the device boundary. The boundary conditions are formulated as follows:

$$\begin{aligned} &S_1 = S_{\text{eq}}\,, \qquad S_2 = 0\,, \qquad \hat{\mathbf{n}} = (0, \cos\theta, \sin\theta)\,, \\ &\hat{\mathbf{m}}\text{: undefined}, \quad \theta = 2\pi x y (1-y)\,, \\ &(x,y) \in \partial([0,1]\times[0,1])\,. \end{aligned} \tag{22}$$

In words, the twist angle θ is zero everywhere except the right-hand-side boundary ($x = 1$) where it quadratically varies between 0 at the ends and $\frac{\pi}{2}$ in the middle. Since the domain width Δx is 1, the twist $\theta/\Delta x$ along the line $y = \frac{1}{2}$ is $\frac{\pi}{2}$, which matches the permanent twist q_0 of the chiral nematic considered, see Eq. (20). Consequently, the elastic free-energy density is minimum along this line, and therefore also the melting of the LC should be the least in this region. Exactly that may be observed in the results from this example, as illustrated in Figures 7 and 8. The largest elastic distortions and hence the greatest S_1-reduction from its equilibrium value of 0.6 appear in the two regions close to the right-hand-side corners of the problem domain. The more interesting outcome from this example, however, is the computed variation of the biaxial part of the resulting Q-tensor field, namely S_2 and $\hat{\mathbf{m}}$ shown in Figure 8. A defect-like state can be detected near $\mathbf{x} = [\frac{3}{4}, \frac{1}{2}]$ around the point of vanishing order parameter S_2, effectively indicating a uniaxial state there. Furthermore, the director field $\hat{\mathbf{m}}$ is a complicated combination of both twist and splay/bend, even though the corresponding field $\hat{\mathbf{n}}$ is mostly a twist/bend with the same handedness throughout the domain.

6 Conclusions

Reported in this paper is a successful attempt to implement a new method of numerical modelling of nematic liquid crystal devices with higher accuracy and computational efficiency while maintaining the high degree of complexity of the underlying mathematical model. For the first time in LC-modelling, the domain mesh has been abandoned in favour of a novel, mesh-free approach to solving the partial differential equations describing LCDs. The method applied here to the Q-tensor

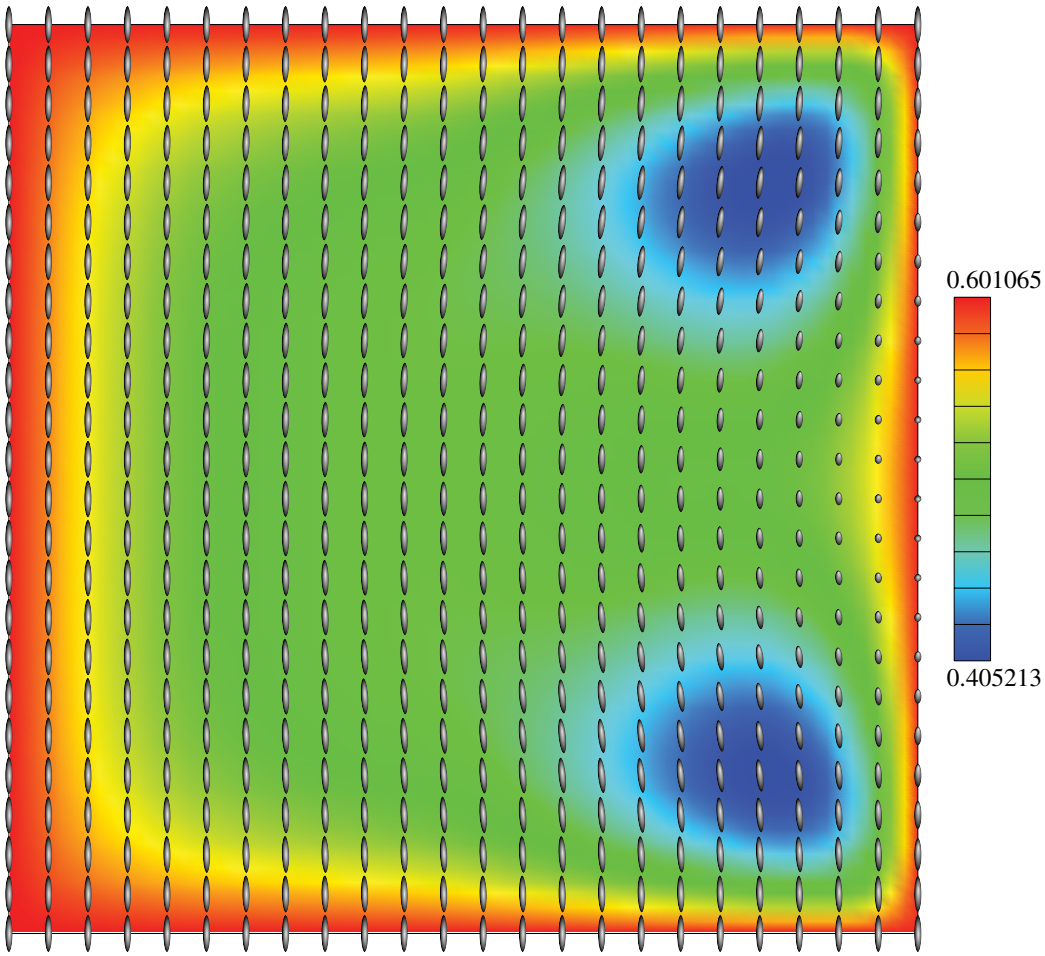

Figure 7 : Resulting profiles of S_1 and $\hat{\mathbf{n}}$ obtained by solving Example 2.

equations of nematostatics is the meshless local Petrov-Galerkin method, which has the potential to compete with the traditional finite difference and finite element methods.

In the theoretical part of the paper, the fundamentals of liquid crystal modelling, such as the descriptive tensor quantity $\mathbf{Q}$ and the energies governing any LC-system, have been discussed. Total-energy minimisation leads to a set of five nonlinear PDEs accompanied by Dirichlet-type boundary constraints of strong LC-anchoring at the liquid crystal surface. MLPG solution of this mathematical model is achieved by formulating the discrete local weak form of a generalised version of the five PDEs and performing a node-collocation process that produces the final system of nonlinear algebraic equations. The Newton-Krylov solution of the algebraic system is the meshfree numerical minimiser of the total static energy in an LC-device.

The presented solution procedure of the meshless local Petrov-Galerkin method is not explained here in its full extent. Various details, such as those of the MLS technique or of the specialised Gaussian cubature formulae, are left out from this paper, but can be found elsewhere, [Breitkopf, Rassineux, Touzot, and Villon (2000), Pecher (2005)]. On the other hand, the procedure is described in terms of a general form of the PDE, not necessarily limited to the particular energies in liquid crystal devices. The procedure also deviates from other MLPG descriptions in certain details, e.g. the way of setting up sizes of the MLS support domains.

The practical demonstration of the MLPG's potential for solving the Q-tensor equations of nematostatics is illustrated by two example problems. The first problem involves a splay/bend-induced topological defect in an achiral nematic LC, while the second problem represents a chiral nematic LC subjected to a twist variation

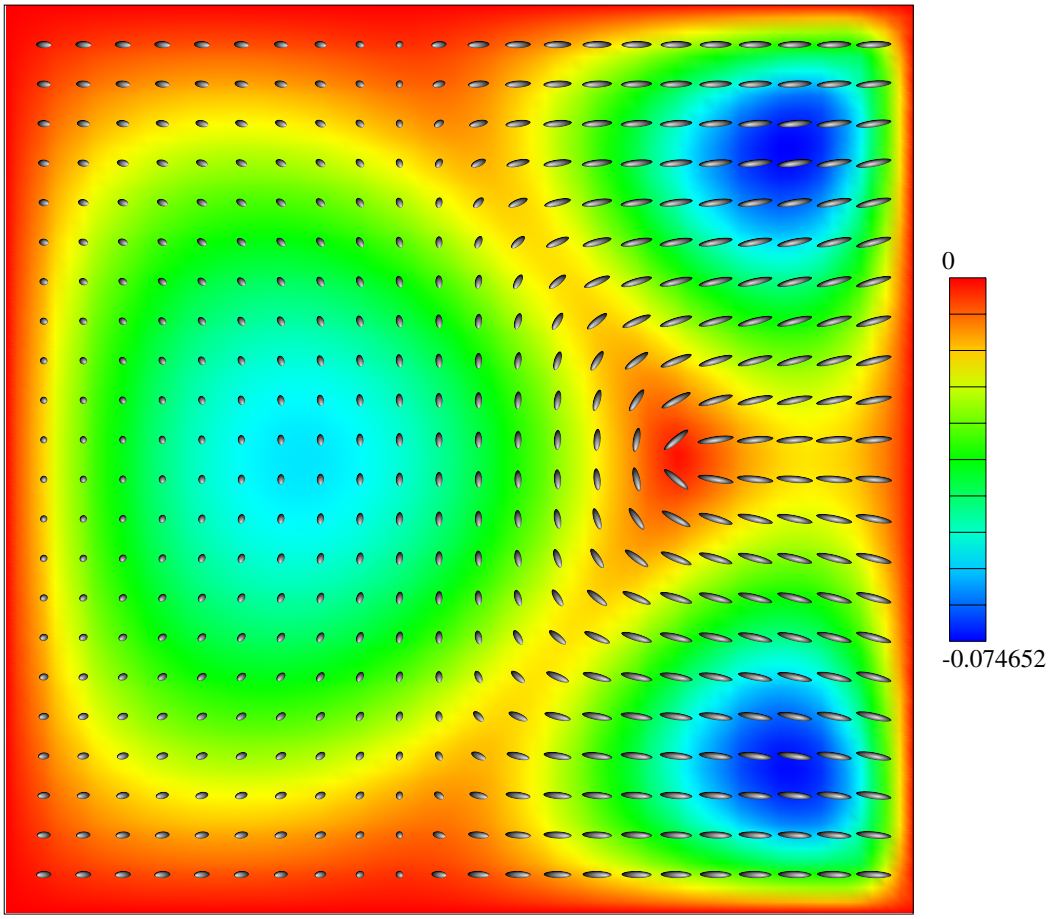

Figure 8 : Resulting profiles of S_2 and $\hat{\mathbf{m}}$ obtained by solving Example 2.

along one of the boundaries. The MLPG solution of the two problems, based on just 576 nodes and 4 cubature points per node, takes less than a minute on a PC and appears correct according to both trends and values across the computational domain. Although the complexity of the mathematical model prevents analytical solutions for comparison purposes, the accuracy of the numerical solutions may be presumed high, based on the overall smoothness and locally large curvature of the resulting profiles. Considering the arbitrarily distributed nodes in both examples, the full power of the meshfree approach to modelling LC-devices will almost certainly exceed the capabilities of the present mesh-based methods when the MLPG nodes are allowed to adapt themselves to the solution.

Formulation of an efficient algorithm for the adaptive nodes' re-distribution in a multi-region domain with curved boundaries is one of the future directions of our research work. Another important extension of the present model is the implementation of additional contributions to the total energy, such as the dielectric, flexoelectric and surface energies. Still another major planned improvement is the introduction of time-dependence into the model, and a further addition of flow effects, eventually solving the so-called Beris-Edwards [Beris and Edwards (1994)] equations of nematodynamics.

Acknowledgement: This work was sponsored by the Engineering and Physical Sciences Research Council and the COMIT Faraday Partnership as part of the Dual Mode Liquid Crystal Displays research programme.

References

Atluri, S.; Shen, S. (2002): *The Meshless Local Petrov-Galerkin (MLPG) Method*. Tech Science Press.

Atluri, S.; Han, Z.D.; and Rajendran, A.M. (2004): A New Implementation of the Meshless Finite Volume Method, Through the MLPG "Mixed" Approach *CMES: Computer Modeling in Engineering & Sciences*, vol. 6, no. 6, pp. 491–514.

Atluri, S.; Zhu, T. (1998): A new meshless local Petrov-Galerkin (MLPG) approach in computational mechanics. *Computational Mechanics*, vol. 22, pp. 117–127.

Beris, A.; Edwards, B. (1994): *Thermodynamics of Flowing Systems with Internal Microstructure - Oxford Engineering Science Series*. Oxford University Press, Oxford.

Berreman, D.; Meiboom, S. (1984): Tensor representation of Oseen-Frank strain energy in uniaxial cholesterics. *Physical Review A*, vol. 30, pp. 1955–1959.

Breitkopf, P.; Rassineux, A.; Touzot, G.; Villon, P. (2000): Explicit form and efficient computation of MLS shape functions and their derivatives. *International Journal for Numerical Methods in Engineering*, vol. 48, pp. 451–466.

de Gennes, P.; Prost, J. (1993): *The Physics of Liquid Crystals (2nd edn), The International Series of Monographs on Physics*. Clarendon Press, Oxford.

Frank, F. (1958): On the theory of liquid crystals. *Discussions of the Faraday Society*, vol. 25, pp. 19–28.

Landau, L.; Lifshitz, E. (1980): *Statistical Physics (3rd edn)*. Pergamon Press, Oxford.

Li, Q.; Shen, S.; Han, Z.; Atluri, S. (2003): Application of meshless local Petrov-Galerkin (MLPG) to problems with singularities, and material discontinuities, in 3-D elasticity. *CMES: Computer Modeling in Engineering & Sciences*, vol. 4, pp. 571–585.

Liu, G. (2003): *Mesh Free Methods: Moving Beyond the Finite Element Method*. CRC Press.

Mori, H.; Gartland, E.; Kelly, J.; Bos, P. (1999): Multidimensional director modeling using the Q tensor representation in a liquid crystal cell and its application to the π cell with patterned electrodes. *Japanese Journal of Applied Physics – Part 1*, vol. 38, pp. 135–146.

Oseen, C. (1933): The theory of liquid crystals. *Transactions of the Faraday Society*, vol. 29, pp. 883–899.

Pecher, R. (2005): Efficient cubature formulae for MLPG and related methods. *International Journal for Numerical Methods in Engineering*, vol. 65, pp. 566–593.

Schopohl, N.; Sluckin, T. (1987): Defect core structure in nematic liquid crystals. *Physical Review Letters*, vol. 59, pp. 2582–2584.